

# Evaluation of Blood-Brain Barrier Integrity by the Analysis of Dynamic Contrast-Enhanced MRI – a Comparison of Quantitative and Semi-Quantitative Methods

David KALA<sup>1,2</sup>, Vlastimil ŠULC<sup>3</sup>, Anna OLŠEROVÁ<sup>3</sup>, JAN SVOBODA<sup>1</sup>, Yeva PRYSIAZHNIUK<sup>1</sup>, Antonín POŠUSTA<sup>1</sup>, Martin KYNČL<sup>4</sup>, Jan ŠANDA<sup>4</sup>, Aleš TOMEK<sup>3</sup>, Jakub OTÁHAL<sup>1,5</sup>

<sup>1</sup>Laboratory of Developmental Epileptology, Institute of Physiology of the Czech Academy of Sciences, Prague, Czech Republic, <sup>2</sup>Faculty of Electrical Engineering, Czech Technical University in Prague, Czech Republic, <sup>3</sup>Department of Neurology, Second Faculty of Medicine, Charles University and University Hospital Motol, Prague, Czech Republic, <sup>4</sup>Department of Radiology, Second Faculty of Medicine, Charles University and University Hospital Motol, Prague, Czech Republic, <sup>5</sup>Department of Pathophysiology, Second Faculty of Medicine, Charles University, Czech Republic

Received June 9, 2022

Accepted October 17, 2022

## Summary

Disruption of the blood-brain barrier (BBB) is a key feature of various brain disorders. To assess its integrity a parametrization of dynamic magnetic resonance imaging (DCE MRI) with a contrast agent (CA) is broadly used. Parametrization can be done quantitatively or semi-quantitatively. Quantitative methods directly describe BBB permeability but exhibit several drawbacks such as high computation demands, reproducibility issues, or low robustness. Semi-quantitative methods are fast to compute, simply mathematically described, and robust, however, they do not describe the status of BBB directly but only as a variation of CA concentration in measured tissue. Our goal was to elucidate differences between five semi-quantitative parameters: maximal intensity ( $I_{max}$ ), normalized permeability index ( $NPI$ ), and difference in DCE values between three timepoints: baseline, 5 min, and 15 min ( $\Delta_{5-0}$ ,  $\Delta_{15-0}$ ,  $\Delta_{15-5}$ ) and two quantitative parameters: transfer constant ( $K^{trans}$ ) and an extravascular fraction ( $Ve$ ). For the purpose of comparison, we analyzed DCE data of four patients 12-15 days after the stroke with visible CA enhancement. Calculated parameters showed abnormalities spatially corresponding with the ischemic lesion, however, findings in individual parameters morphometrically differed.  $K^{trans}$  and  $Ve$  were highly correlated.  $\Delta_{5-0}$  and  $\Delta_{15-0}$  were prominent in regions with rapid CA enhancement and highly correlated with  $K^{trans}$ . Abnormalities in  $\Delta_{15-5}$  and  $NPI$  were more homogenous with

less variable values, smoother borders, and less detail than  $K^{trans}$ . Moreover, only  $\Delta_{15-5}$  and  $NPI$  were able to distinguish vessels from extravascular space. Our comparison provides important knowledge for understanding and interpreting parameters derived from DCE MRI by both quantitative and semi-quantitative methods.

## Key words

DCE MRI • Time-intensity curve • Blood-brain barrier • Stroke • Toft's model

## Corresponding authors

D. Kala, Laboratory of Developmental Epileptology, Institute of Physiology of the Czech Academy of Sciences, Vídeňská 1083, 142 20 Prague 4, Czech Republic. E-mail: david.kala@fgu.cas.cz and J. Otáhal, Laboratory of Developmental Epileptology, Institute of Physiology of the Czech Academy of Sciences, Vídeňská 1083, 142 20 Prague 4, Czech Republic. E-mail: jakub.otahal@fgu.cas.cz

## Introduction

The blood-brain barrier (BBB) is a functional structure formed by endothelial cells of the brain non-fenestrated capillaries, basal lamina, astrocytes, and

pericytes. It serves as an interface between the vascular and extracellular space of the central nervous tissue (i.e. separates blood components from nervous tissue). Thus, it plays a fundamental role in the maintenance of brain homeostasis and normal neuronal function. Disruption of the BBB followed by the leakage of blood components into the extracellular space is, however, a key feature of various brain disorders including tumors [1], cerebral ischemia [2], multiple sclerosis [3], small vessel diseases [4], Alzheimer's disease [5] or diabetes [6]. Evaluation of the BBB integrity is thus an important diagnostic step to set an appropriate diagnosis and justified the treatment.

To assess the BBB integrity magnetic resonance imaging (MRI) after an application of an MRI contrast agent (CA) is broadly used. The presence of CA in the scanned tissue shortens its T1 relaxation time and thereby causes enhancement (increased intensity) in T1w (T1-weighted MRI) images. The enhancement is observed in all regions where CA has been distributed. In MRI measurement continuous space of brain tissue is virtually divided into discrete regularly distributed spatial elements called voxels. Every voxel has a defined location (in 3D space), intensity of the measured MRI signal, and all voxels have the same volume. The volume of a voxel is based on the scanner resolution and ranges

typically between the units of cubic millimeters and the hundreds of cubic microns. Although a resolution of MRI allows good macroscopic (anatomic) resolution to distinguish white and gray matter, each voxel has its microscopic structure which is below the resolution of the scanner. In the case of neuronal tissue, a typical voxel is composed of different cellular elements (neurons, astrocytes, oligodendrocytes, etc.) and vessels with unknown proportions. This leads to the phenomenon called the partial volume effect, where a voxel is composed of several compartments and the measured signal is a result of the convolution of signals from all compartments of the voxel. If the voxel is composed of a single compartment such as blood the signal deviation after administration of CA can be converted to R1 relaxation rate and then is proportional to the concentration of CA within the blood. In nonhomogeneous voxels, such as those within the brain tissue, the mechanism of signal deviation after the administration of CA is more complex and typically depends on blood volume, the volume of extracellular space, and permeability of the blood-tissue interface i.e. blood-brain barrier within the voxel. Several scenarios which result in signal enhancement within the voxel after CA injection are shown in Figure 1.

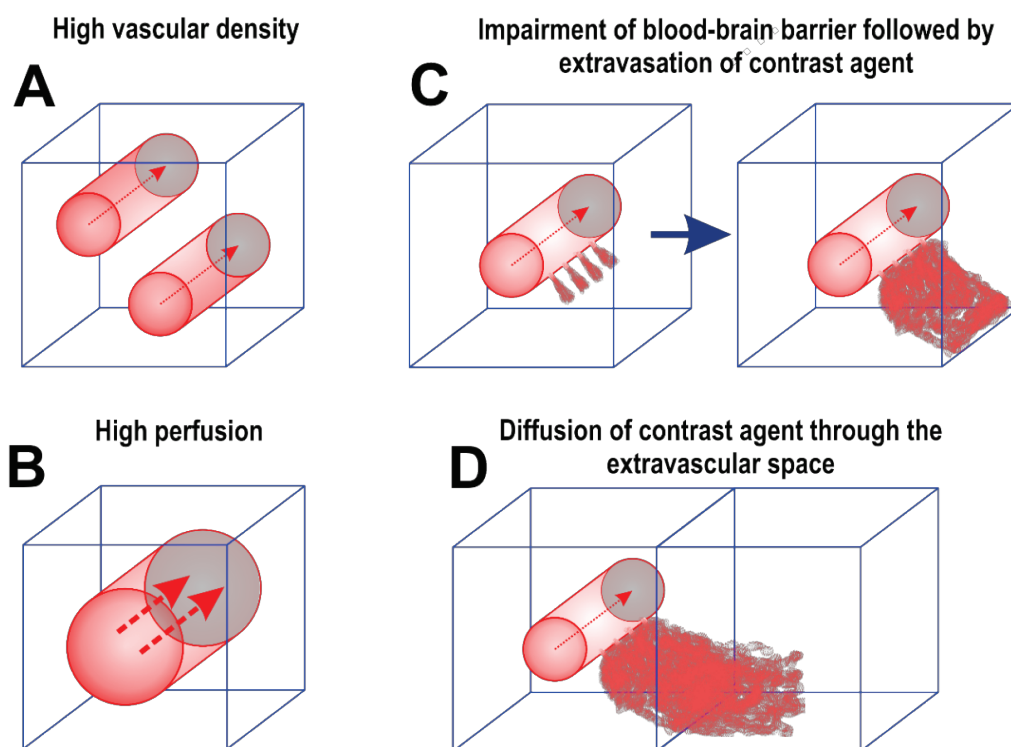


**Fig. 1.** Basic (patho)physiological principles manifest as an enhancement of DCE intensity. Only in C and D, however, the BBB is disrupted. In reality, several principles take effect at the same time. A measured DCE signal is then formed as a combination of all participating principles.

When the BBB is impaired, various substances including CA can pass the vascular wall in both directions [7-10]. The direction and speed of the CA movement across the barrier depend on the severity of BBB impairment and driving forces (pressure, concentration, and osmotic gradients between the blood and the extracellular space) [11-13]. Moreover, CA that crosses the BBB within one voxel can diffuse by the bulk flow through the extravascular space further to the surrounding voxels [14]. The T1w signal deviation in this case thus corresponds to the overall amount of CA in both vascular and extravascular compartments within the voxel [15]. Therefore, if the BBB integrity is compromised, time becomes an important factor in the assessment of signal deviations [16-19]. In common clinical practice, a pair of static scans are acquired i.e. before and after contrast agent application [20]. This approach obviously does not allow quantitative estimation of blood-brain barrier impairment and the conclusion would only declare contrast enhancement within the region [21,22]. However, to elucidate the proportions of sources of signal enhancement algorithms based on the analysis of time-intensity curves (TICs), where every TIC describes the development of T1w intensity in the voxel over time, have been developed [23,24] (for review see [25]). The particular shape of each TIC reflects the specific combination of compartments within the voxel and their pathophysiological conditions.

To obtain TICs a dynamic MRI sequence has to be employed. The most commonly used dynamic MRI sequence for TICs acquisition is called dynamic contrast-enhanced MRI (DCE). During the DCE, a CA is injected intravenously while T1-weighted (T1w) MRI brain scans are continually acquired with desired frequency before, during, and after CA administration. The shape of TICs usually follows a specific pattern within specific time windows after the CA injection, i.e. phases of TIC [26,27]. The early TIC phase usually lasts for the first five minutes after the CA injection. During this period a rapid DCE intensity enhancement is observed inside well-perfused regions, as well as early signs of hemorrhage or extravasation across impaired BBB, could be visible. As the effect of BBB impairment on TIC shape is prominent during the early phase, it has been the main interest of most DCE analysis methods so far. TICs then continuously decline in regions with intact BBB during the late phase which lasts from approximately five minutes after CA application up to the end of MRI acquisition (~ twenty minutes after CA injection). In

several pathologies (e.g. Alzheimer's disease, dementia, or multiple sclerosis) the disruption of BBB is only subtle and hidden by noise in the early TIC phase. However, as CA continues to slowly flow across impaired BBB to the extravascular tissue it causes a slow elevation of TIC also during the late phase. The content of CA in extracellular space is attributed to BBB breakdown [28], however, active mechanisms such as transcytosis were recently suggested [29]. The analysis of TIC in the late phase proved to be beneficial in the detection of subtle changes in BBB integrity and its importance was emphasized in recent studies [30,31].

There are three main approaches to how TICs can be analyzed: qualitatively, quantitatively, or semi-quantitatively [21]. The qualitative approach is based on visual observation of either 4D MRI images (3D and time axes) or individual TICs. Both require a skilled radiologist and provide biased results. Their use is limited to fast on-spot detection of tissue with abnormal behavior as part of the diagnostic process in clinical practice.

The goal of the quantitative approach is, on the other hand, to describe the tissue properties (i.e. blood perfusion, the status of BBB, tissue composition, etc.) by quantitative parameters. Those properties are estimated by fitting individual TICs (within each voxel) of DCE-MRI by a pharmacokinetic model [25], a mathematical equation that describes the relationship between those properties and measured DCE intensity change. There are several existing pharmacokinetic models varying in the number of tissue compartments and definition of model parameters (for review see [32,33]). In this study, we have used the Toft's two-compartment model [34], one of the simpler but still commonly used model. Toft's model fits the DCE data using two parameters  $K^{trans}$ ; a transfer constant between blood plasma and extracellular space per unit of volume and time and  $Ve$ ; a fraction of extracellular-extravascular space per unit volume ( $Ve$ ).

Quantitative DCE analysis using pharmacokinetic models became the current golden standard [21], although, there has been still no consensus on the model selection and, moreover, it exhibits several drawbacks. First of all, fitting the large DCE-MRI data by the model is a computationally demanding and time-consuming procedure [24]. Secondly, most of the current pharmacokinetic models require prior knowledge of arterial input function (AIF) – i.e. the signal in input arteries. The measurement of AIF was, however, recognized as a key source of error in DCE modeling and

no consensus about the method of proper acquisition of AIF has been made so far [35-38]. Lastly, concerns about the objectivity of the DCE fitting method were raised as it suffers from significant variability of the results based on the used scanner [39], fitting model [40], or acquisition protocol [41]. It was also shown that only in 25 % of voxels the quality of the fit was robust enough for the reproducible clinical evaluation of the data (for a full review of Toft's model reliability see [42]).

The last approach to the analysis of DCE-MRI is the semi-quantitative method. Instead of fitting the data, it uses a mathematical description of individual TICs by parameters that express the main features of the curve's dynamics and shape. Avoiding the fitting procedure, semi-quantitative methods do not suffer from the drawbacks of high computational demand and low fit robustness. On the other hand, the parameters obtained by the semi-quantitative analysis do not directly cohere with specific tissue properties and thus provide only an indirect description of the underlying tissue physiology.

The goal of this study is to qualitatively and spatially compare  $K^{trans}$ , one of the standard model-based quantitative parameters, with other less demanding semi-quantitative parameters and evaluate how those parameters can be interpreted. Moreover, we will compare  $K^{trans}$ , as a parameter of the early TIC phase, with three parameters of the late TIC phase to elucidate the relations between parameters describing a different time period after CA injection.

## Methods

In this study, we have examined four patients 12-15 days after cerebral ischemia when under normal scenario patient are typically discharged from hospital care. It has been shown previously that BBB impairment after the stroke might persist beyond this time point (for review see [13]). Patients were examined by specially designed MRI protocol, which consists of anatomical scans for detection of the ischemic lesion and DCE MRI for the evaluation of BBB. DCE time series of each patient were further processed by quantitative and semi-quantitative analyses of time-intensity curves for every voxel.

### Participants

Four patients, two males (66 and 70 years old) and two females (71 and 80 years old) after cerebral ischemia in the middle cerebral artery territory were used

in this study. All patients were treated according to the current guidelines on acute stroke treatment [20] and all patients underwent successful mechanical recanalization within the therapeutic time frame. The study was approved by the Ethics Committee of University Hospital Motol (Ref. number: EK-1091/14) and all patients signed informed consent.

### MR imaging

MRI examination was performed 12-15 days after the ischemic insult using Siemens 3T Vida Magnetom scanner. MRI protocol consists of structural MRI: T1weighted (T1w; relaxation time TR 2400 ms, echo time TE 2.29 ms, flip angle FA 8°, voxel size 0.8×0.8×0.8 mm, duration 6:47 min), Fluid Attenuation Recovery (FLAIR; TR 6000 ms, TE 390 ms, TI 1900 ms, variable FA, voxel size 1×1×0.9 mm, duration 7:20 min), Susceptibility weighted (SWI; TR 28 ms, TE 20 ms, FA 15°, voxel size 0.6×0.6×2 mm, duration 4:42 min); quantitative T1 (qT1) measured by the method of two variable flip angles (TR 15 ms, TE 2 ms, FA 4° and 23°, voxel size 1×1×1 mm, duration 4:20 min); Diffusion MRI (DWI; TR 5300 ms, TE 97 ms, voxel size 2×2×2 mm, b [0,1000,3000], 20 directions, duration 4:42 min); dynamic contrast enhanced MRI (DCE; TR 3.6 ms, TE 1.34 ms, FA 9°, voxel size 2×2×2 mm, time resolution 5 s, 36 repetitions with the total duration of 3 min); dynamic susceptibility contrast (DSC; TR 1500 ms, TE 27 ms, FA 90°, voxel size 2×2×3 mm, time resolution 1.5 s, 80 repetitions with the total duration of 2:08 min); and another two short DCE MRI (TR 3.6 ms, TE 1.34 ms, FA 9°, voxel size 2×2×2 mm, time resolution 5 s, 5 repetitions with a duration of 30 s each) for analysis of late phase.

A total volume of 15 ml (bodyweight (BW) <75 kg) or 20 ml (BW ≥75 kg) of contrast agent (Gadovist, Gadobutrol 1 mmol/ml, Bayer Pharma AG, Germany) was administered to the patient in a two-phase scheme [43]. First, 1/3 of CA (5 or 7.5 according to BW) was injected 30 s after initiation of the DCE sequence. Remaining CA (10 or 12.5 according to BW) was injected during the DSC sequence, specifically 10 s after its initiation. DSC followed right after the DCE sequence. The injections were performed into the left arm *via* the 22-gauge cannula that was catheterized prior to the examination. Five and fifteen minutes after CA injection, respectively, another two short DCE sequences were acquired. No additional CA was injected during those sequences.

### MRI preprocessing

All MRI sequences were registered to the common anatomical space of the T1w image and thereafter normalized into standard MNI (Montreal Neurological Institute template) space by the SPM12 MATLAB toolbox. During the normalization step, all non-brain structures (i.e. skull, muscles, skin, and cerebral fluid) were removed. FLAIR and DWI (calculated from diffusion MRI) images were used for the manual outline of the ischemic lesion by a skilled radiologist. SWI protocol was used for the exclusion of bleeding and hemorrhagic transformation.

### Quantitative and semi-quantitative analysis of DCE

In this study, TICs of all brain voxels were extracted and parametrized by the set of commonly used quantitative and semi-quantitative parameters. Quantitative parameters  $K^{trans}$  and  $Ve$ , and semi-quantitative parameters  $Imax$  and  $\Delta_{5-0}$  were used for the description of the early TIC phase (0-5 min after CA administration). Semi-quantitative parameters  $\Delta_{15-5}$ ,  $\Delta_{15-0}$ , and  $NPI$  (normalized permeability index) were used for the description of the late TIC phase (5-15 min after CA administration).

Quantitative parameters ( $K^{trans}$  and  $Ve$ ) were derived from the early TIC phase (a rapid DCE intensity enhancement due to the fast arrival of the CA bolus) by a fitting of individual TICs by a multi-compartment pharmacokinetic model, namely original Toft's model [44]. For the fitting, the ROCKETSHIP Matlab tool [45] was used. To convert the DCE signal to residual function  $R_f$  quantitative T1 map (map of T1 relaxation times of each voxel) obtained by the method of two variable flip angles (FA 4° and 23°) was used inside the ROCKETSHIP. The arterial input function (AIF) a prerequisite for the fitting procedure has been derived from voxels exhibiting the fastest and steepest TIC which anatomically corresponded to the lumen of the middle cerebral artery (MCA) [36-38]. Obtained parameters  $K^{trans}$  and  $Ve$  are quantitative, i.e. have a clear physical interpretation.  $K^{trans}$  ( $\text{min}^{-1}$ ) is defined as a transfer constant and describes the balance between capillary permeability and blood flow [34].  $Ve$  is a fraction of the volume of extracellular space per unit volume of tissue and is usually written either in ml/100 ml or in unitless form.

Two semi-quantitative parameters, that also describe the early TIC phase,  $Imax$  and  $\Delta_{5-0}$  were calculated using the in-house Matlab script. The  $Imax$

parameter is defined as the maximal value of TIC during the first DCE part. Parameter  $\Delta_{5-0}$  is defined as a difference between the baseline and TIC average intensity during 2<sup>nd</sup> DCE (measured 5 min after the CA injection). The baseline intensity was calculated as an average of the first five consecutive scans of the 1<sup>st</sup> DCE MRI (before the CA was injected).

$$\Delta_{5-0} = \frac{\sum_{t=1}^N I_{2ndDCE}}{N} - Baseline \quad 1$$

$$Baseline = \frac{\sum_{t=1}^5 I_{1stDCE}}{5} \quad 1$$

Where N is the number of time points of the corresponding DCE part (in our case N=5, see acquisition protocol) and  $I_{1stDCE}$ ,  $I_{2ndDCE}$ , and  $I_{3rdDCE}$  are the signal intensity of the corresponding TIC during 1<sup>st</sup>, 2<sup>nd</sup>, and 3<sup>rd</sup> DCE part, respectively.

To describe the late TIC phase, three semi-quantitative parameters  $\Delta_{15-0}$ ,  $\Delta_{15-5}$ , and  $NPI$  were calculated. Parameters  $\Delta_{15-0}$  and  $\Delta_{15-5}$  are defined as the differences between TIC average intensity during 3<sup>rd</sup> DCE (15 min) and baseline, and between 3<sup>rd</sup> (15 min) and 2<sup>nd</sup> (5 min) DCE, respectively. Parameter  $NPI$  (normalized permeability index [31]) is defined as a ratio between  $\Delta_{15-5}$  calculated from the TIC of the observed tissue and TIC corresponding to sagittal sinus (venous input function, VIF).

$$\Delta_{15-0} = \frac{\sum_{t=1}^n I_{3rdDCE}}{N} - Baseline \quad 2$$

$$\Delta_{15-5} = \frac{\sum_{t=1}^{N_3} I_{3rdDCE}}{N_3} - \frac{\sum_{t=1}^{N_2} I_{2ndDCE}}{N_2} \quad 3$$

$$NPI = \frac{\Delta_{15-5}}{\Delta_{15-5}(VIF)} \quad 4$$

Where  $N_2$  and  $N_3$  are the numbers of time points of the 2<sup>nd</sup> and 3<sup>rd</sup> DCE part, respectively, and,  $I_{2ndDCE}$  and  $I_{3rdDCE}$  are the signal intensity of the corresponding TIC during those parts.

### Evaluation of the contrast between the lesion and healthy tissue

Masks of ischemic pathology were manually outlined on FLAIR and DWI images by a skilled radiologist. The ischemic lesion was then defined as a unification of both obtained masks (FLAIR  $\cup$  DWI, Fig. 2). To evaluate how individual TIC parameters change between the ischemic lesion and healthy tissue, the ischemic mask was mirrored to the second hemisphere and its contralateral projection was created. Median values of individual TIC parameters inside the ischemic lesion and its contralateral projection were then

calculated. Finally, the relative change of those median values was assessed (Equation 5) and averaged across all patients for the purpose of statistical comparison (Equation 6).

$$\delta_Q(P) = \frac{\text{median}(Q(P)(x,y,z)^{\text{lesion}}) - \text{median}(Q(P)(x,y,z)^{\text{contralateral}})}{\text{median}(Q(P)(x,y,z)^{\text{contralateral}})} \quad 5$$

$$\Phi_Q = \text{mean}(\delta_Q(P)) \quad 6$$

$\delta_Q$  is the relative change between median values of the lesion and its contralateral projection for TIC DCE parameter Q and is calculated for each patient P separately.  $\Phi_Q$  is an average relative change of TIC DCE parameter Q across all patients.

#### Evaluation of spatial characteristics of TIC parameters

The abnormalities in individual maps of TIC parameters were segmented using the thresholding technique. The threshold values were manually determined for each map and each patient individually to achieve the best separation of parameter abnormality from the unchanged (healthy) tissue. The volume of detected abnormality was then calculated and for the purpose of inter-subject comparability divided by the volume of the ischemic lesion (detected in FLAIR or DWI) of the corresponding patient as described in Equation 7.

$$\text{normalized volume}_Q(P) = \frac{\text{volume}_Q(P)}{\text{volume}_{\text{FLAIR} \cup \text{DWI}}(P)} \quad 7$$

Where Q is an indication of individual TIC parameters for patient P.

To describe the variability of the individual TIC parameters within the ischemic lesion relative standard deviation (standard deviation divided by the mean value) of all voxels of the ischemic/contralateral region was calculated.

Moreover, for the assessment of detailed spatial properties of TIC parameters twenty line profiles (LP) (five profiles per patient) across the ischemic lesion for every map of each TIC parameter were manually outlined. As individual parameters have different units and scales, all line profiles were first normalized ( $LP_{\text{norm}}$ ) to a 0-1 scale according to Equation 8 or 10 in case of *NPI*. Finally, the coastline index (CI) was calculated from each normalized profile by Equation 10 as a characteristic of the amount of detail in the profile.

$$LP_{\text{norm}_n} = \frac{I_n - \min_n I_n}{\max_n I_n - \min_n I_n}, n = 1, 2, \dots, M \quad 8$$

$$LP_{\text{norm}}(NPI)_n = \frac{|I_n - \max_n I_n|}{\max_n |I_n - \max_n I_n|}, n = 1, 2, \dots, M \quad 9$$

Where  $I_n$  (arbitrary units a.u.) is a single intensity of line-profile  $I$  in sample  $n$ ,  $M$  (number of samples) is the length of the line profile, and  $\min_n$  and  $\max_n$  are operands for minimal and maximal intensity value of line profile, respectively.

$$CI = \frac{\sum |LP_{\text{norm}_n} - LP_{\text{norm}_{n-1}}|}{M}, n = 2, 3, \dots, M \quad 10$$

Where CI is the coastline index,  $I_n$  is the value of the intensity profile in sample  $n$ , and  $M$  is the length of the intensity profile.

## Results

In this study, we have compared quantitative and semi-quantitative methods for the analysis of DCE. Two standard quantitative parameters  $K^{\text{trans}}$  and  $Ve$  derived from Toft's model were confronted with their semi-quantitative alternatives  $Imax$  and  $\Delta_{5-0}$  calculated from the early phase and also with  $\Delta_{15-0}$ ,  $\Delta_{15-5}$ , and *NPI* extracted from the late phase of the TIC (median values of individual parameters from all patients are shown in Fig. 3B).

A complete set of all obtained TIC parameter maps for one representative patient is provided in Figure 3A. In this patient, a large ischemic lesion in the left MCA territory possesses an abnormality in all TIC parameter maps. The location of the TIC abnormality (contrast enhancement) corresponds with the location of the ischemic lesion (depicted in Fig. 2). The spatial correlation of TIC parameter abnormalities (of all parameters) with ischemic lesions was observed in every patient recruited to the study. Figure 3A also demonstrates that, although individual alterations of TIC parameter color-maps spatially correspond with the ischemic lesion, they differ in morphology, size, and intensity.

To further evaluate the relation between all derived TIC parameters twenty line profiles (five per patient) across the ischemic lesion were manually drawn and values of TIC parameters were obtained (Fig. 4A-B). Correlation coefficients between pairs of parameters were calculated for each profile and then averaged for a patient. The final correlation matrix elucidating the relation between all parameters is shown in Figure 4C.

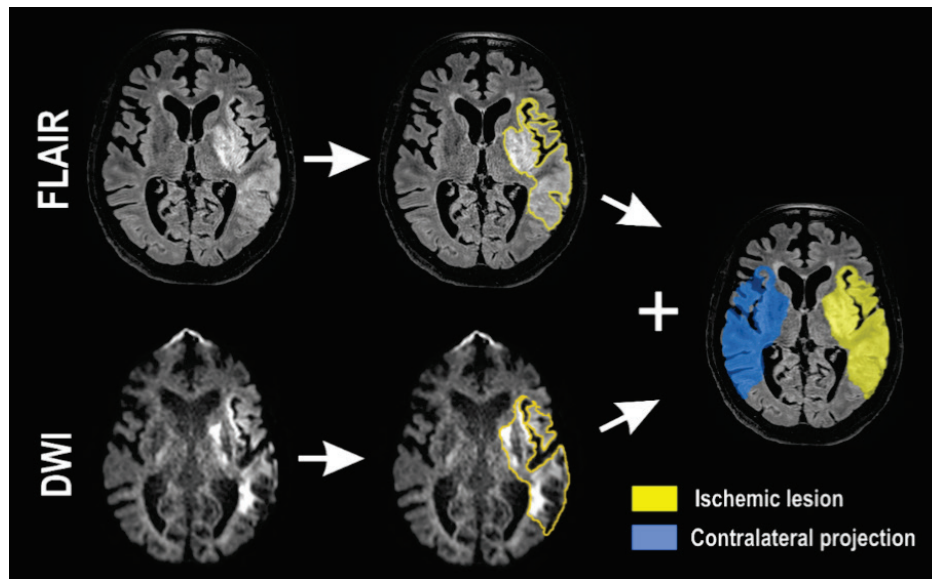


**Fig. 2.** An example patient with left-sided cerebral ischemia (on the right side of the MRI image). The masks of ischemic tissue were manually outlined on FLAIR and DWI MRI scans. The final mask of the whole ischemic lesion was then created as a unification of FLAIR and DWI masks. For comparison of the lesion with healthy tissue, the mask of the ischemic lesion was mirrored across the interhemispheric line to create its contralateral projection in the healthy hemisphere.

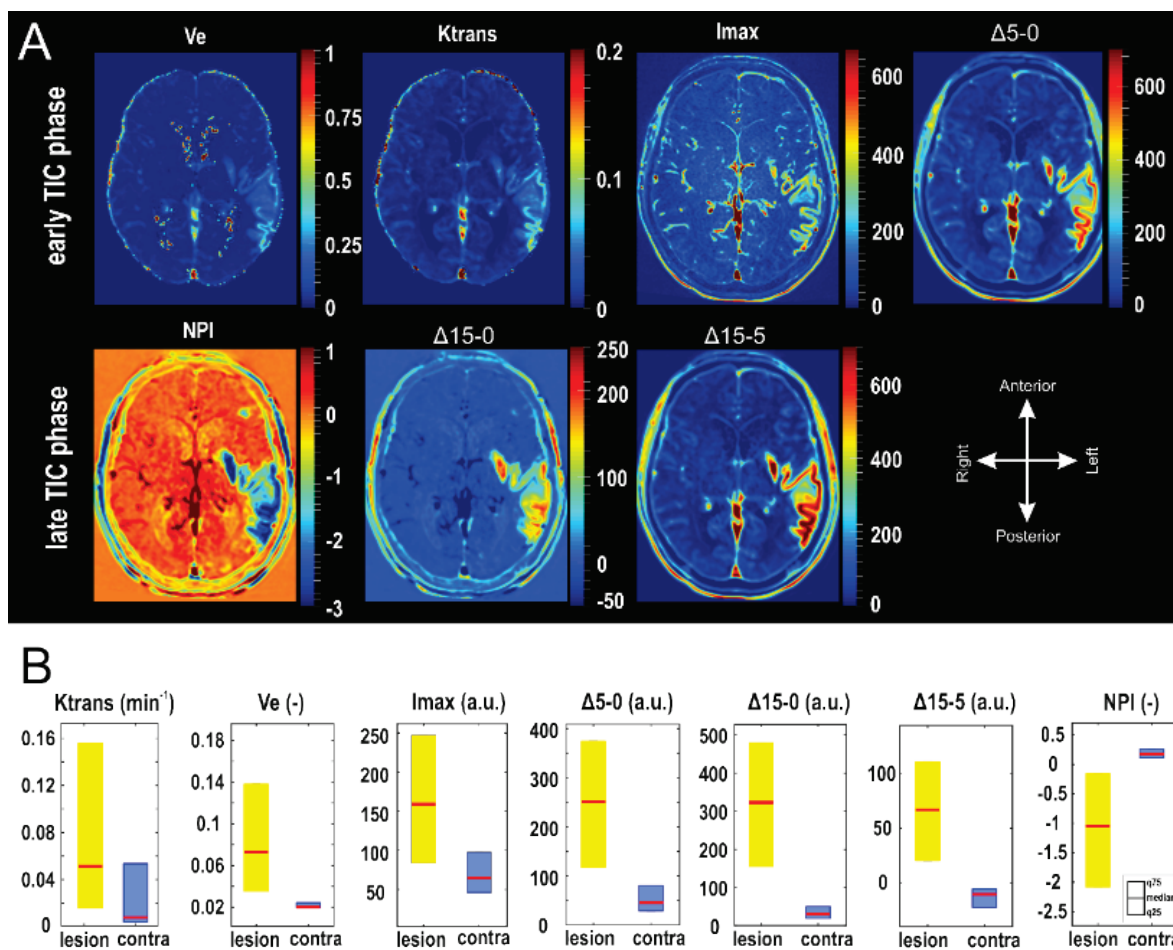


**Fig. 3.** (A) TIC parameter maps calculated in a representative patient from DCE obtained 13 days after mechanical recanalization of left MCA. A large ischemic lesion is depicted in the left MCA territory. (B) Values of TIC parameters inside ischemic lesion and in its contralateral projection were calculated from all patients. (a.u.) arbitrary units, (-) unitless.

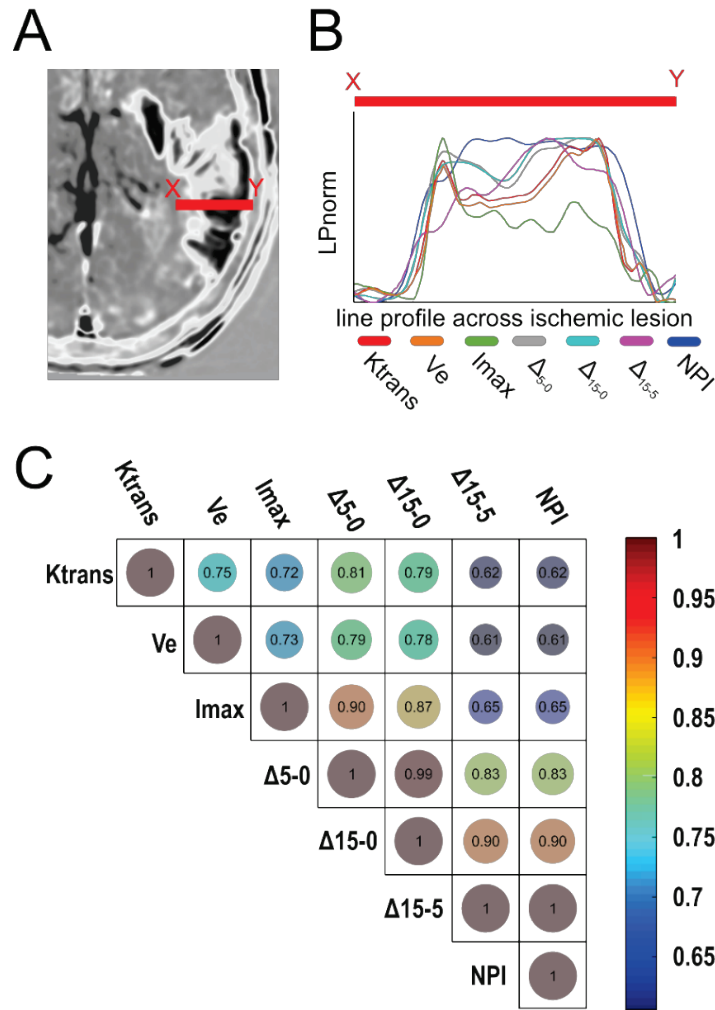


**Fig. 4.** (A-B) Normalized line profiles of all individual TIC parameters calculated across the ischemic lesion in the same representative patient as in Figure 3. (C) An averaged correlation matrix between individual DCE TIC parameters along line profiles drawn across the lesion derived from all recruited patients.

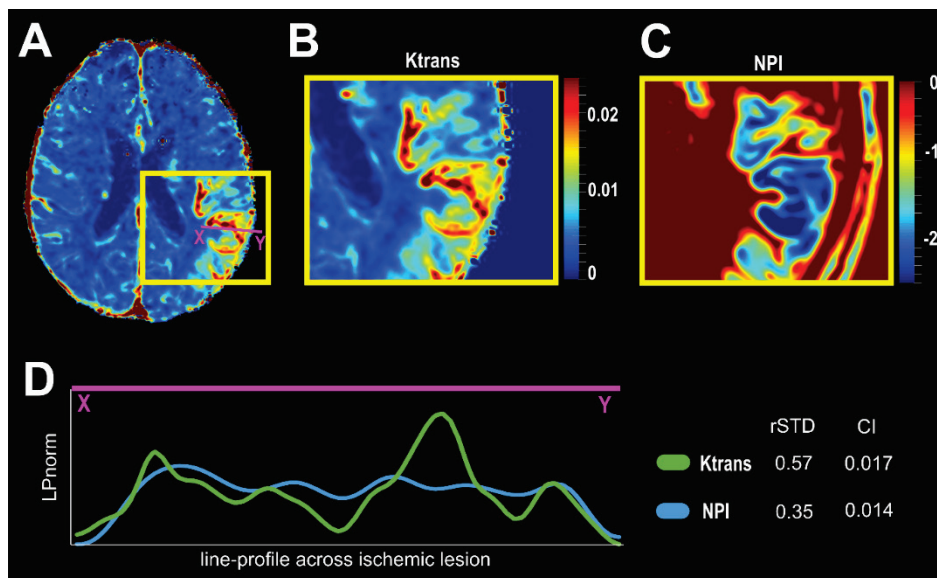


**Fig. 5.** (A-C)  $K^{trans}$  parameter inside the ischemic lesion is more variable and therefore shows more spatial resolution than *NPI*. (D) An example of one line profile drawn across the ischemic lesion for  $K^{trans}$  and *NPI* DCE TIC parameters and corresponding values of rSTD (relative standard deviation) and CI (coastline index) characteristics.

The correlation matrix shows that both quantitative parameters  $K^{trans}$  and  $Ve$  behaved in tight correlation (0.75,  $p < 0.001$ ). Correlation has been found also between semi-quantitative and quantitative parameters. However, the lowest correlation of  $NPI$  to other semi- and quantitative parameters had been observed. The possible mechanisms are discussed further in the discussion.

By visual observation of complete image datasets, spatial differences between parameters were visible and likely caused by two factors. Firstly, by the different variability of parameter values along the profile, and secondly, by the varying spatial extension of abnormality visible in color maps of individual parameters (Fig. 5). To describe the source of variability between the parameters more thoroughly, four mathe-

matical characteristics per parameter were evaluated. The variability of parameter values within the visible abnormality was tested by calculation of relative standard deviation (rSTD) of values of the individual parameters inside the ischemic lesion, and also by calculation of coastline index (CI) of parameter line profiles across the ischemic lesion. The volume of abnormality visible in individual parameter color maps was evaluated for the description of spatial differences. Moreover, a variable contrast between abnormality and healthy tissue detected on color maps of individual parameters was observed. This variability was assessed by calculating the median difference between parameter values inside the ischemic lesion and inside its contralateral projection. All characteristics for individual parameters are summarized in Table 1 and graphically demonstrated in Figure 6.

**Table 1.** Average values of evaluated spatial characteristics of TIC parameters. Values are presented as mean  $\pm$  S.E.M.

Parameter	Contrast between ischemic lesion and healthy tissue (-) *	Normalized volume (-)	Relative STD in the lesion (-)	Coastline index (-)
$K^{trans}$	2.8 $\pm$ 1.00	0.48 $\pm$ 0.11	0.81 $\pm$ 0.10	0.017 $\pm$ 0.002
$Ve$	3.6 $\pm$ 0.93	0.26 $\pm$ 0.04	0.79 $\pm$ 0.09	0.017 $\pm$ 0.001
$Imax$	1.57 $\pm$ 0.24	0.22 $\pm$ 0.04	0.32 $\pm$ 0.01	0.021 $\pm$ 0.002
$\Delta_{5-0}$	5.4 $\pm$ 1.42	0.32 $\pm$ 0.05	0.42 $\pm$ 0.06	0.014 $\pm$ 0.001
$\Delta_{15-0}$	11.3 $\pm$ 1.35	0.34 $\pm$ 0.06	0.39 $\pm$ 0.05	0.013 $\pm$ 0.001
$\Delta_{15-5}$	-7.2 $\pm$ 1.61	0.30 $\pm$ 0.05	0.43 $\pm$ 0.07	0.014 $\pm$ 0.001
$NPI$	-7.3 $\pm$ 1.64	0.37 $\pm$ 0.05	0.47 $\pm$ 0.19	0.014 $\pm$ 0.001

\* Calculated as relative change of parameters between the lesion and the contralateral hemisphere. (-) unitless.

First, we have compared the quantitative parameter  $K^{trans}$  with semi-quantitative parameters of the early TIC phase. Parameter  $\Delta_{5-0}$  is defined as a difference between TIC value 5 min after CI injection and the baseline. High values of  $\Delta_{5-0}$  suggest voxels with a high fraction of well-perfused vessels or extravascular tissue with heavy leakage across the BBB. The parameter manifests absolute changes in CA concentration, however, it did not describes its dynamics. In our study,  $\Delta_{5-0}$  behaved in close correlation with  $K^{trans}$  (0.81,  $p < 0.001$ ). It had significantly lower rSTD inside ischemic lesion (0.43 vs. 0.82,  $p = 0.004$ ), significantly higher contrast between lesion and healthy tissue (4.43 vs. 2.41,  $p = 0.043$ ), and non-significantly lower CI (0.014 vs. 0.017,  $p = 0.550$ ), however, similar normalized volume of detected abnormality (0.32 vs. 0.47,  $p = 0.300$ ).

The second compared semi-quantitative

parameter of the early TIC phase was  $Imax$ , which represents the maximal intensity of TIC during the early TIC phase. The highest intensities of TIC, i.e. the highest concentration of CA in a measured voxel, is present in vascular space. Therefore vessels are prominent on  $Imax$  color maps. In comparison with  $K^{trans}$ ,  $Imax$  had lower correlation (0.73,  $p < 0.001$ ), significantly lower rSTD (0.33 vs. 0.82,  $p = 0.017$ ), and not differed in contrast between healthy and abnormal tissue (1.37 vs. 2.41,  $p = 0.280$ ), CI (0.015 vs. 0.013,  $p = 0.823$ ) and normalized volume of detected abnormality (0.21 vs. 0.47,  $p = 0.141$ ).

Further, we have compared  $K^{trans}$  with three parameters of the late TIC phase. Parameter  $\Delta_{15-0}$  is defined as a difference between TIC intensities 15 min after CI injection and the baseline. It describes the dominant increase of TIC intensity during the early TIC phase caused by the rapid entrance of CA into the blood

system, but in comparison with  $\Delta_{5-0}$ , it also describes more subtle changes in TIC intensity caused by the slow transport of CA across the BBB. In comparison with  $K^{trans}$ , parameter  $\Delta_{15-0}$  behaved in the highest correlation of all parameters of the late TIC phase (0.79,  $p < 0.001$ ), it had a significantly lower rSTD (0.43 vs. 0.82,  $p = 0.007$ ),

significantly higher contrast between healthy and abnormal tissue (11.01 vs. 2.41,  $p = 0.009$ ), significantly lower CI (0.013 vs. 0.017,  $p = 0.023$ ), and did not significantly differ in normalized volume of detected abnormality (0.34 vs. 0.47,  $p = 0.402$ ).

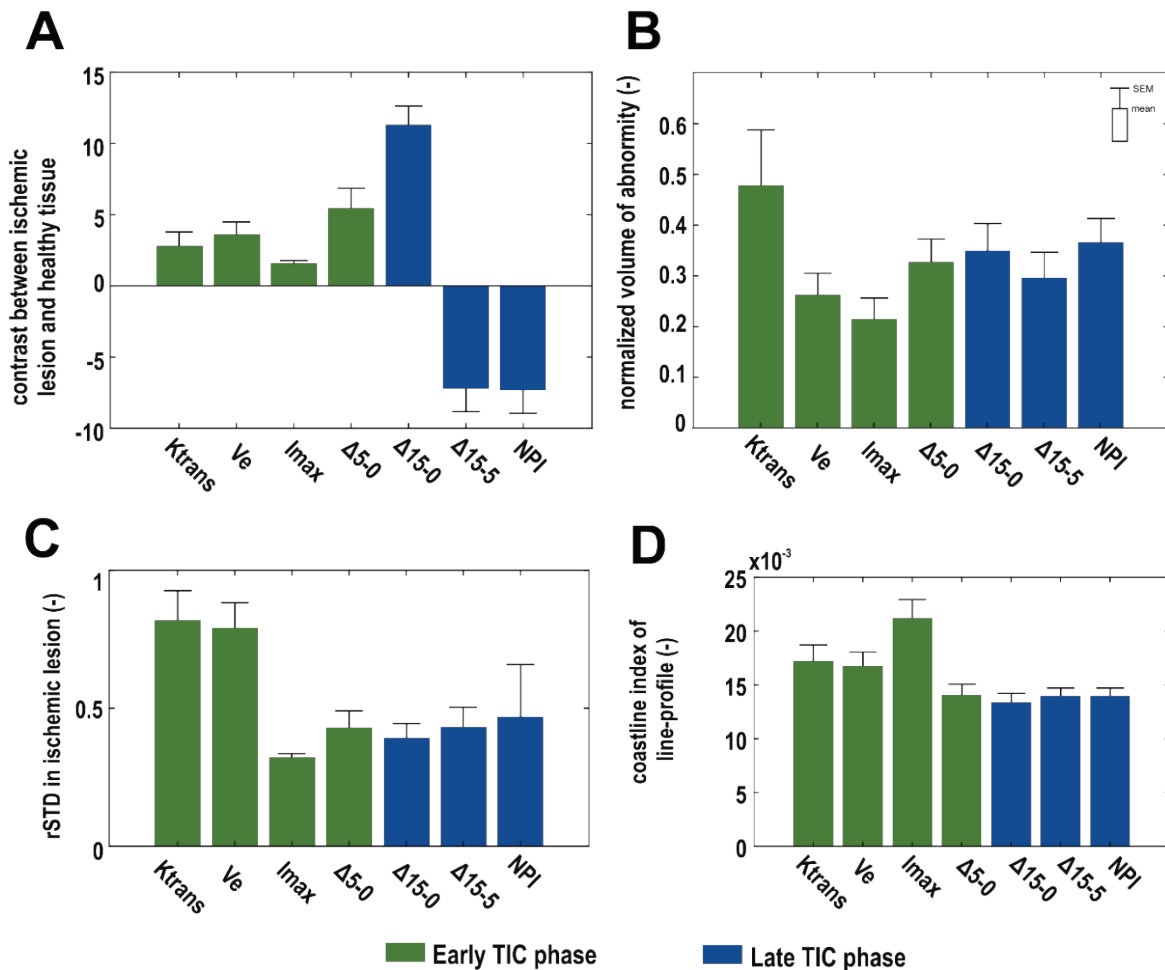


**Fig. 6.** Comparison of parameters describing early and late TIC phase by four characteristics. Bars represent mean and error bars S.E.M.

Parameter  $\Delta_{15-5}$  describes the difference in TIC intensities 15 and 5 min after CA injection. It follows the slow dynamic of CA in the tissue. Two main patterns of dynamics can be distinguished. In the case of vascular compartments with intact BBB, a slow decline of TIC intensity is observed as the level of CA in the blood decrease due to excretion. In this case, values of  $\Delta_{15-5}$  are negative (as the intensity in 15 min is lower than in 5 min time point). When BBB is impaired, the slow transition of CA into the extracellular compartment can cause an increase in TIC intensity resulting in the positive value of  $\Delta_{15-5}$ . However, a combination of both processes is present and therefore parameter  $\Delta_{15-5}$  serves as

an important indicator showing which of those factors is dominant in the tissue. In our study, parameter  $\Delta_{15-5}$  in comparison with  $K^{trans}$  behaved in lower correlation (0.62,  $p < 0.001$ ), it had significantly lower rSTD (0.43 vs. 0.82,  $p = 0.006$ ), significantly higher contrast between healthy and abnormal tissue (-8.73 vs. 2.41,  $p = 0.036$ ) and significantly lower CI (0.014 vs. 0.017,  $p = 0.036$ ). It did not significantly differ in normalized volume of detected abnormality (0.29 vs. 0.47,  $p = 0.220$ ).

The last evaluated parameter was  $NPI$ .  $NPI$  is derived from  $\Delta_{15-5}$  by normalization of its values by values measured in large veins such as superior sagittal sinus. After the normalization, the effect of a global trend

in the vascular compartment (usually slow decline of CA concentration due to excretion) on the TIC intensity is suppressed. *NPI*, therefore, should be more sensitive to changes in TIC intensity caused by BBB impairment although other sources of positivity such as hyperemia cannot be excluded. The sign of the *NPI* parameter defines the direction of TIC in its late phase in comparison to the direction of TIC used for normalization, i.e. signal from a large vessel. Positive *NPI* means the same TIC direction as in the vein, and negative *NPI* the opposite direction. As the direction of TIC in veins is in the majority of cases negative caused by the decrease of CA concentration, positive values of *NPI* suggest the decrease of CA concentration, on the other hand, negative *NPI* suggests accumulation of CA in the measured voxel. The correlation of the *NPI* parameter with  $K^{trans}$  in our study was the lowest (0.62,  $p < 0.001$ ), it had a significantly lower rSTD (0.47 vs. 0.82,  $p = 0.034$ ),

significantly higher contrast between healthy and abnormal tissue (-8.76 vs. 2.41,  $p = 0.036$ ), and significantly lower CI (0.014 vs. 0.017,  $p = 0.036$ ). It did not significantly differ in normalized volume of detected abnormality (0.36 vs. 0.47,  $p = 0.422$ ).

To visualize the results of the semi-quantitative DCE evaluation in the vascular compartment a dataset where a large artery and ischemic lesion with CA enhancement are visible together (Fig. 7). Although brain vessels and ischemic region are both visible with good contrast on T1w image after the application of CA, only  $\Delta_{15-5}$  and *NPI* (late phase TIC derived parameters) distinguish between vessel i.e. vascular compartment and brain tissue with obviously impaired BBB. Contrarily, *Imax*,  $\Delta_{5-0}$ , and  $\Delta_{15-0}$  (i.e. parameters derived from the early phase of TIC) do not provide the possibility to differentiate vessels (vascular compartment) from brain tissue with CA enhancement.

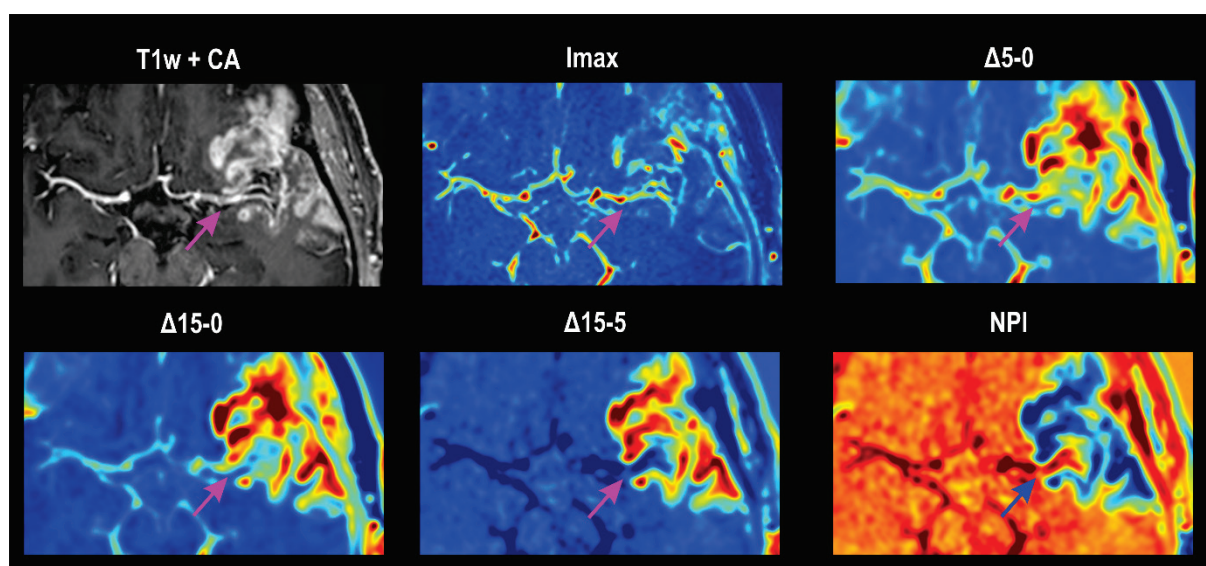


**Fig. 7.** A visual comparison of semi-quantitative TIC parameters in the region where brain vessels are present together with contrast enhancement within brain tissue. Brain vessel (marked by an arrow) is clearly visible in T1w image after CA. Parameters  $\Delta_{15-5}$  and *NPI* can distinguish between vessel and brain tissue with impaired BBB. Contrary with parameters *Imax*,  $\Delta_{5-0}$ , and  $\Delta_{15-0}$  it is not possible to differentiate vessels from brain tissue with CA enhancement.

## Discussion

In this study, we have spatially compared TIC-derived quantitative parameters  $K^{trans}$  and  $V_e$  obtained by the Toft's model with semi-quantitative parameters *Imax* and  $\Delta_{5-0}$  describing the early TIC phase, and parameters  $\Delta_{15-0}$ ,  $\Delta_{15-5}$ , and *NPI* describing the late TIC phase. Although semi-quantitative parameters do not provide quantitative measures of BBB and might be affected by partial volume effect they do not require

demanding curve fitting for their calculation and can be thus used more broadly in contrast to the quantitative ones [24]. It was also shown that semi-quantitative parameters describing the late TIC phase proved to be beneficial in the detection of subtle changes in BBB integrity, however, their results should be interpreted with caution due to the partial volume effect [27]. In this study, we have selected a set of semi-quantitative parameters that can describe the whole TIC trajectory (both early and late phase) with the aim to evaluate how

those parameters can be interpreted and how they spatially differ from model-based parameters  $K^{trans}$  and  $Ve$ .

We have calculated both quantitative and semi-quantitative TIC parameters in four patients 12-15 days after cerebral ischemia. Values of all parameters significantly differ inside the ischemic lesion in comparison with the contralateral healthy hemisphere. This correlates with findings made by Villringer *et al.* [46], who shows 3-4 times higher  $K^{trans}$  values in the ischemic lesion in comparison to healthy tissue. Also, spatial correlation of ischemic lesion with abnormalities detected in color maps of TIC parameters was observed in all patients. However, individual parameters differ in morphology, size, and intensity of the detected abnormality.

To elucidate the differences between individual TIC parameters, twenty line profiles across the ischemic lesion were drawn with the aim to cover all important patterns visually observed inside lesions. For the purpose of comparability, values of all TIC parameters along the line profiles were normalized to the 0-1 range and the cross-correlation matrix of normalized profiles was calculated. Figure 4C shows that  $NPI$  and  $\Delta_{15.5}$  behaved identically in this comparison. The source of this behavior is in the combination of  $NPI$  definition, where  $NPI$  is calculated from  $\Delta_{15.5}$  by dividing it by the signal from veins, and 0-1 normalization that annuls the previous normalization. Both parameters had therefore the same results, however, normalization of  $NPI$  by venous signal makes it more suitable for the inter-subject comparison. It should be, however, noted that although normalization by the vascular signal is performed in  $NPI$  calculation it does not fully withdraw vascular function within the voxel and thus positive findings on the  $NPI$  could be caused by the increased volume of the vascular compartment such as during the hyperemia.

Further, to evaluate the spatial differences between individual parameters more closely, we have calculated four spatial characteristics: coastline index, relative standard deviation, relative change inside the ischemic lesion, and volume of detected abnormality.

The coastline index (CI) was used for the description of variability along the line profiles and the relative standard deviation (rSTD) of parameter values inside the whole ischemic lesion was calculated to extend the knowledge about parameter variability to larger volume (not only in line profile as in the case of CI). Both higher CI and higher rSTD suggest more variable parameter values that provides a more detailed

description of parameter changes along the ischemic lesion. However, whether the source of the detail is caused by higher sensitivity of the parameter to tissue changes or by a higher presence of noise cannot be distinguished by our analysis. This is a clear limitation of this study.

Further, we have assessed the relative change of parameter values (parameter contrast) inside the ischemic lesion and in the contralateral hemisphere. This characteristic describes the ability of a parameter to distinguish between healthy and impaired tissue. As abnormalities detected in individual parameter colormaps differ also in size, we have also compared the total volume of detected abnormality in all patients and parameters.

Parameters  $K^{trans}$ ,  $Ve$ ,  $Imax$ , and  $\Delta_{5.0}$  describe the early change of TIC after CA bolus injection.  $K^{trans}$  is dependent primarily on the slope of initial signal increase however  $Ve$  on TIC peak value [47]. The correlation of those two independent parameters was 0.75. Parameter  $\Delta_{5.0}$  describes the difference of TIC values before CA injection and during plateau after the initial peak. It had a similar correlation with  $K^{trans}$  (0.81) and  $Ve$  (0.79) suggesting, that  $\Delta_{5.0}$  is dependent on both, the slope of the initial TIC increase and TIC peak value. We have observed no significant difference between spatial characteristics of  $\Delta_{5.0}$  and  $K^{trans}$ . Parameter  $\Delta_{5.0}$  shows a similar pattern as  $K^{trans}$ , it does not require dynamic scanning (only a few samples of baseline and signal 5 min after CA injection) or data fitting and therefore can be easily measured and calculated. However,  $\Delta_{5.0}$  lacks the ability of  $K^{trans}$  to quantitatively describe the BBB permeability and therefore is without further normalization less suitable for inter-subject comparison. However, it has to be emphasized, that variations in  $\Delta_{5.0}$  (and also other semi-quantitative parameters) are a representation of CA concentration in the total volume of the measured voxel, and do not necessarily represent the BBB disruption. This fact should be always considered in interpretations based on semi-quantitative parameters.

Parameter  $Imax$ , by its definition, describes the maximal values of TIC and therefore highlights the tissue with the highest concentration of CA. Therefore, we had expected a dominant correlation between  $Imax$  and  $Ve$  (that is also primarily dependent on TIC peak value). However, in our study,  $Imax$  correlated with  $Ve$  (0.73) in the same way as with the  $K^{trans}$  (0.72). By visual observation abnormalities in the  $Imax$  map highly correlated with vessels while it had significantly lower

values outside them. This can explain the lower correlation to the  $Ve$  that by the definition shows high values in tissue with high extravascular-extracellular space. It also describes the low volume of abnormality detected in  $I_{max}$  maps.

Parameter  $\Delta_{15-0}$  is defined as the difference between values of the baseline (before CA injection) and TIC values 15 min after CA. As so, it contains information about both, the initial TIC increase and the following slow transition (either decrease or increase in case of CA accumulation). We have observed a high correlation (0.99) of  $\Delta_{15-0}$  with  $\Delta_{5-0}$ . As  $\Delta_{5-0}$  is calculated only from the early part of TIC it can be assumed that the effect of the initial increase is also dominant in  $\Delta_{15-0}$  drowning the effect of subtle late TIC transition. Therefore it carries no extra information and has no extra advantage or drawback than those described for  $\Delta_{5-0}$ .

In comparison with other used parameters,  $\Delta_{15-5}$ , and  $NPI$ , describe the late TIC phase only. In the line profile correlation analysis they behave identically due to the normalization of line profile values as discussed above. The correlation of both late TIC phase parameters with other parameters of the early TIC phase was lower (0.65  $K^{trans}$ , 0.61  $Ve$ , and 0.65  $\Delta_{5-0}$ ). The important difference between parameters of the early and late TIC phase is, that in the case of the late TIC phase (15 min after CA injection), there is enough time for CA to leak out of the vessels and diffuse to surrounding regions. In comparison with  $K^{trans}$ , the detected abnormality is then more homogenous with less variable values, smoother borders, though, with less detail about the tissue structure (represented by observed significantly lower CI and rSTD), and more contrast (significantly higher contrast between ischemic and healthy tissue). On the other hand, early TIC phase parameters more closely reflect the changes in the tissue composition as the transitions between voxels mainly filled by vessels and extravascular voxels are more sudden and clearly distinguishable. For those reasons, we emphasize the use of late TIC parameters for the complex description of BBB status.

We have also tested the ability of semi-quantitative TIC parameters to distinguish extravascular tissue from clearly visible vessels. Figure 7 demonstrates that only  $NPI$  and  $\Delta_{15-5}$  were able to distinguish those types of tissue. This is caused by the fact, that each parameter describes a different aspect of TIC.  $NPI$  and  $\Delta_{15-5}$  both describe the slow transition of TIC signal in the late phase. In vessels, this transition appears in form of a slow decrease, however, in extravascular tissue with

impaired BBB in form of a slow increase caused by the accumulation of CA. In case of other parameters, the underlying aspects are similar in vessels and extravascular tissue, and therefore, they are not able to distinguish those types of tissue.

Parameter  $K^{trans}$  is a transfer constant between blood plasma and extracellular space. However, it emphasized that the  $K^{trans}$  is a combination of permeability-surface area (PS) and blood flow; i.e. it does not rely on BBB permeability only. It approximates permeability in the situation when blood flow is much larger than PS, however, in other scenarios are individual effects of PS and blood flow hardly separable [48].

In this study, we have used basic Toft's model as it is one of the computationally simplest deriving two parameters. Figure 8A shows time concentration curves (that were calculated from DCE TICs during the fitting procedure), their fit curves by Toft's model, and corresponding values of  $K^{trans}$  and  $Ve$ . Concentration and fit curves are provided for three representative tissues: healthy tissue, ischemic lesion, and sagittal sinus. It is obvious that Toft's model was able to clearly separate all representative tissues. However, simple Toft's model uses a function with only two parameters for fitting DCE TICs. Together with the low temporal resolution of the DCE sequence, it leads to a time shift in a fit of both regions similarly as can be visible in Figure 8A. Figure 8B provides single line profiles of  $K^{trans}$  values across the ischemic lesion in one representative patient derived from three different pharmacokinetic models namely Toft's, extended Toft's, and Patlak model. Although Toft's model overestimates  $K^{trans}$  values in comparison with the other two, their line profiles do not differ spatially. We have also obtained  $Ve$  values in healthy tissue approximately ten times lower than expected according to the literature [49] (Fig. 3B). One of the possible explanations could be the short DCE scanning duration used in our study. Obtained DCE time curves cover mostly the accumulation phase of the CA in the extravascular space, while its return to the intravascular space occurs later. Thus, extravascular space behaves as a compartment with infinite volume making its fractional volume,  $Ve$ , hard to estimate. Although the quantitative values in our study of estimated parameters might be inaccurate we have focused primarily on a spatial comparison of selected methods. In situations, where precise quantification is desired use of a more complex compartment model (Patlak, 2-compartment uptake) should be considered.

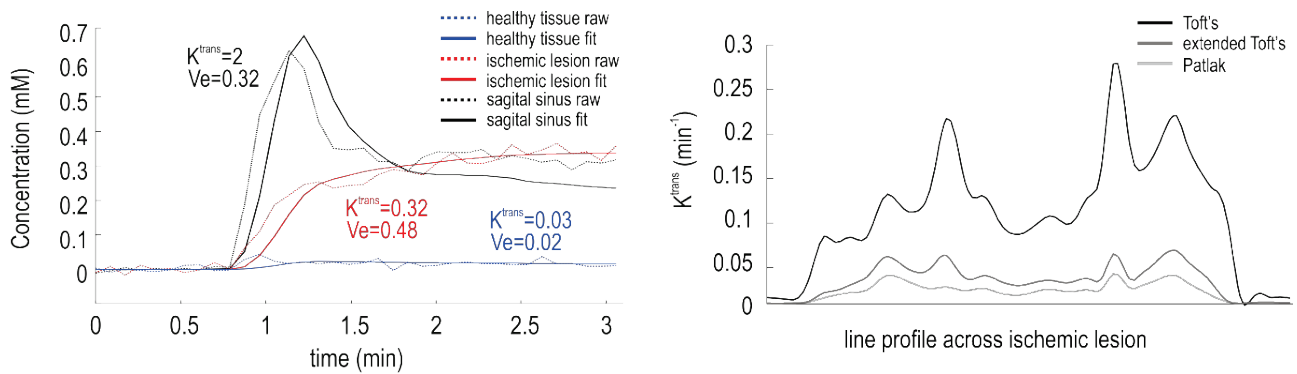


**Fig. 8. (A)** Time curves of CA concentration (calculated from DCE TIC) in three representative voxels (dotted line; healthy tissue in blue, ischemic lesion in red, and sagittal sinus in black) and respective fits by Toft's model (solid line). **(B)** Comparison of line profiles of  $K^{trans}$  values along the ischemic lesion calculated by three different fitting models, Toft's (black), extended Toft's (dark grey), and Patlak model (light grey). Basic Toft's model overestimates  $K^{trans}$  values in comparison with other models, however, spatial characteristics along the ischemic lesion are similar for all models.

In summary, quantitative methods provide quantitative parameters with clear physiological definition, however, they are computationally demanding and suffer from several concerns about their objectivity. Semi-quantitative methods, on the other hand, are easily computed and thus can be used *ad hoc* and also on large datasets. Mathematical description of semi-quantitative parameters is clear with high objectivity, however, they do not have any direct physiological relevance. We have shown a comparison of five semi-quantitative parameters ( $Imax$ ,  $\Delta_{5-0}$ ,  $\Delta_{15-0}$ ,  $\Delta_{15-5}$ , and  $NPI$ ) with one of the standard model-based quantitative parameter ( $K^{trans}$ ). All parameters were able to detect enhancement of CA in tissue after stroke, however, findings in individual parameters morphometrically differ. It has to be emphasized, that for all described semi-quantitative parameters applies, and that increase in parameter value is a representation of CA concentration in the total volume of measured voxel, which does not necessarily represent the BBB disruption. This fact should be always

considered in interpretations based on semi-quantitative parameters.

### Conflict of Interest

There is no conflict of interest.

### Acknowledgements

The project was supported by grants from the Czech Health Research Council numbers NU21-02-00289 and NU21-08-00228. Additional support of this work was provided by the Czech Academy of Sciences within the program "QUALITAS – Wellbeing in Health and Disease" and the IPHYS facility within the MEYS CR (Large RI Project LM2018129 Czech-BioImaging) and by project nr. LX22NPO5107 (MEYS): Financed by EU – Next Generation EU. We especially acknowledge the valuable work of MRI radiological assistants Jan Brhel and Veronika Borovcová, and the technical support by Jaroslav Tintěra.

### References

1. Cuenod CA, Fournier L, Balvay D, Guinebretière JM. Tumor angiogenesis: pathophysiology and implications for contrast-enhanced MRI and CT assessment. *Abdom Imaging* 2006;31:188-193. <https://doi.org/10.1007/s00261-005-0386-5>
2. Merali Z, Huang K, Mikulis D, Silver F, Kassner A. Evolution of blood-brain-barrier permeability after acute ischemic stroke. *PLoS One* 2017;12:1-11. <https://doi.org/10.1371/journal.pone.0171558>
3. Jelescu IO, Leppert IR, Narayanan S, Araújo D, Arnold DL, Pike GB. Dual-temporal resolution dynamic contrast-enhanced MRI protocol for blood-brain barrier permeability measurement in enhancing multiple sclerosis lesions. *J Magn Reson Imaging* 2011;33:1291-1300. <https://doi.org/10.1002/jmri.22565>
4. Thrippleton MJ, Backes WH, Sourbron S, Ingrid M, van Osch MJP, Dichgans M, Fazekas F, ET AL. Quantifying blood-brain barrier leakage in small vessel disease: Review and consensus recommendations. *Alzheimer's Dement* 2019;15:840-858. <https://doi.org/10.1016/j.jalz.2019.01.013>

5. Starr JM, Farrall AJ, Armitage P, McGurn B, Wardlaw J. Blood-brain barrier permeability in Alzheimer's disease: a case-control MRI study. *Psychiatry Res Neuroimaging* 2009;171:232-241. <https://doi.org/10.1016/j.psychresns.2008.04.003>
6. Starr JM. Increased blood-brain barrier permeability in type II diabetes demonstrated by gadolinium magnetic resonance imaging. *J Neurol Neurosurg Psychiatry* 2003;74:70-76. <https://doi.org/10.1136/jnnp.74.1.70>
7. Kastrup A, Engelhorn T, Beaulieu C, De Crespigny A, Moseley ME. Dynamics of cerebral injury, perfusion, and blood-brain barrier changes after temporary and permanent middle cerebral artery occlusion in the rat. *J Neurol Sci* 1999;166:91-99. [https://doi.org/10.1016/S0022-510X\(99\)00121-5](https://doi.org/10.1016/S0022-510X(99)00121-5)
8. Ličeník R, Bednařík J, Tomek A, Bar M, Neumann J, Šaňák D, Nečas T, Bůřilová P, Klugarová J, Pokorná A, Klugar M. Development of Czech National Stroke Guidelines. *Int J Evid Based Healthc* 2019;17(Suppl 1): S9-S11. <https://doi.org/10.1097/XEB.0000000000000190>
9. Harris NG, Gauden V, Fraser PA, Williams SR, Parker GJM. MRI measurement of blood-brain barrier permeability following spontaneous reperfusion in the starch microsphere model of ischemia. *Magn Reson Imaging* 2002;20:221-230. [https://doi.org/10.1016/S0730-725X\(02\)00498-8](https://doi.org/10.1016/S0730-725X(02)00498-8)
10. Durukan A, Marinkovic I, Strbian D, Pitkonen M, Pedrono E, Soinne L, Abo-Ramadan U, Tatlisumak T. Post-ischemic blood-brain barrier leakage in rats: One-week follow-up by MRI. *Brain Res* 2009;1280:158-165. <https://doi.org/10.1016/j.brainres.2009.05.025>
11. On NH, Savant S, Toews M, Miller DW. Rapid and reversible enhancement of blood-brain barrier permeability using lysophosphatidic acid. *J Cereb Blood Flow Metab* 2013;33:1944-1954. <https://doi.org/10.1038/jcbfm.2013.154>
12. Whelan R, Hargaden GC, Knox AJS. Pharmaceuticals modulating the blood-brain barrier: a comprehensive review. *Pharmaceutics* 2021;13:1980. <https://doi.org/10.3390/pharmaceutics13111980>
13. Bernardo-Castro S, Sousa JA, Brás A, Cecília C, Rodrigues B, Almendra L, Machado C, ET AL. Pathophysiology of blood-brain barrier permeability throughout the different stages of ischemic stroke and its implication on hemorrhagic transformation and recovery. *Front Neurol* 2020;11:1605. <https://doi.org/10.3389/fneur.2020.594672>
14. O'Brien MD. Ischemic cerebral edema. A review. *Stroke* 1979;10:623-628. <https://doi.org/10.1161/01.STR.10.6.623>
15. Rodriguez Gutierrez D, Wells K, Diaz Montesdeoca O, Moran Santana A, Mendichovszky IA, Gordon I. Partial volume effects in dynamic contrast magnetic resonance renal studies. *Eur J Radiol* 2010;75:221-229. <https://doi.org/10.1016/j.ejrad.2009.04.073>
16. Knight RA, Dereski MO, Helpern JA, Ordidge RJ, Chopp M. Magnetic resonance imaging assessment of evolving focal cerebral ischemia. Comparison with histopathology in rats. *Stroke* 1994;25:1252-1261; discussion 1261-1262. <https://doi.org/10.1161/01.STR.25.6.1252>
17. Srinivasan A., Goyal M., Al Azri F, Lum C. State-of-the-art imaging of acute stroke. *RadioGraphics* 2006;26(Suppl 1):S75-S95. <https://doi.org/10.1148/rg.26si065501>
18. Milidonis X, Marshall I, Macleod MR, Sena ES. Magnetic resonance imaging in experimental stroke and comparison with histology systematic review and meta-analysis. *Stroke* 2015;46:843-851. <https://doi.org/10.1161/STROKEAHA.114.007560>
19. Lansberg MG, Thijs VN, Brien MWO, Ali JO, Crespigny AJ De, Tong DC, Moseley ME, Albers GW. Evolution of apparent diffusion coefficient, diffusion-weighted, and T2-weighted signal intensity of acute stroke. *AJNR Am J Neuroradiol* 2001;22:637-644.
20. Škoda O, Herzig R, Mikulík R, Neumann J, Václavík D, Bar M, Šaňák D, Tomek A, Školoudík D. Clinical Guideline for the Diagnostics and Treatment of Patients with Ischemic Stroke and Transitory Ischemic Attack - Version 2016. *Česká a Slov Neurol a Neurochir* 2016;79/112:351-363. <https://doi.org/10.14735/amcsnn2016351>
21. Barnes SL, Whisenant JG, Loveless ME, Yankeelov TE. Practical Dynamic Contrast Enhanced MRI in Small Animal Models of Cancer: Data Acquisition, Data Analysis, and Interpretation. *Pharmaceutics* 2012;4: 442-478. <https://doi.org/10.3390/pharmaceutics4030442>

22. Chassidim Y, Vazana U, Prager O, Veksler R, Bar-Klein G, Schoknecht K, Fassler M, Lublinsky S, Shelef I. Analyzing the blood-brain barrier: The benefits of medical imaging in research and clinical practice. *Semin Cell Dev Biol* 2015;38:43-52. <https://doi.org/10.1016/j.semcdb.2014.11.007>
23. Lavini C, de Jonge MC, van de Sande MGH, Tak PP, Nederveen AJ, Maas M. Pixel-by-pixel analysis of DCE MRI curve patterns and an illustration of its application to the imaging of the musculoskeletal system. *Magn Reson Imaging* 2007;25:604-612. <https://doi.org/10.1016/j.mri.2006.10.021>
24. Fabijańska A. A novel approach for quantification of time-intensity curves in a DCE-MRI image series with an application to prostate cancer. *Comput Biol Med* 2016;73:119-130. <https://doi.org/10.1016/j.compbiomed.2016.04.010>
25. Sourbron SP, Buckley DL. Tracer kinetic modelling in MRI: Estimating perfusion and capillary permeability. *Phys Med Biol* 2012;57:R1-R33. <https://doi.org/10.1088/0031-9155/57/2/R1>
26. Jones EF, Sinha SP, Newitt DC, Klifa C, Kornak J, Park CC, Hylton NM. MRI enhancement in stromal tissue surrounding breast tumors: Association with recurrence free survival following neoadjuvant chemotherapy. *PLoS One* 2013;8:e61969. <https://doi.org/10.1371/journal.pone.0061969>
27. Veksler R, Vazana U, Serlin Y, Prager O, Ofer J, Shemen N, Fisher AM, ET AL. Slow blood-to-brain transport underlies enduring barrier dysfunction in American football players. *Brain* 2020;143:1826-1842. <https://doi.org/10.1093/brain/awaa140>
28. Haar HJ, Jansen JFA, Jeukens CRLPN, Burgmans S, Buchem MA, Muller M, Hofman PAM, ET AL. Subtle blood-brain barrier leakage rate and spatial extent: Considerations for dynamic contrast-enhanced MRI. *Med Phys* 2017;44:4112-4125. <https://doi.org/10.1002/mp.12328>
29. Yang AC, Stevens MY, Chen MB, Lee DP, Stähli D, Gate D, Contrepois K, ET AL. Physiological blood-brain transport is impaired with age by a shift in transcytosis. *Nature* 2020;583:425-430. <https://doi.org/10.1038/s41586-020-2453-z>
30. van den Kerkhof M, Voorter PHM, Canjels LPW, de Jong JJA, van Oostenbrugge RJ, Kroon AA, Jansen JFA, Backes WH. Time-efficient measurement of subtle blood-brain barrier leakage using a T1 mapping MRI protocol at 7T. *Magn Reson Med* 2021;85:2761-2770. <https://doi.org/10.1002/mrm.28629>
31. Veksler R, Vazana U, Serlin Y, Prager O, Ofer J, Shemen N, Fisher AM, ET AL. Slow blood-to-brain transport underlies enduring barrier dysfunction in American football players. *Brain* 2020;143:1826-1842. <https://doi.org/10.1093/brain/awaa140>
32. Khalifa F, Soliman A, El-Baz A, Abou El-Ghar M, El-Diasty T, Gimel'Farb G, Ouseph R, Dwyer AC. Models and methods for analyzing DCE-MRI: A review. *Med Phys* 2014;41:124301. <https://doi.org/10.1118/1.4898202>
33. Barnes SR, Ng TSC, Montagne A, Law M, Zlokovic BV, Jacobs RE. Optimal acquisition and modeling parameters for accurate assessment of low K<sub>trans</sub> blood-brain barrier permeability using dynamic contrast-enhanced MRI. *Magn Reson Med* 2016;75:1967-1977. <https://doi.org/10.1002/mrm.25793>
34. Tofts PS, Brix G, Buckley DL, Evelhoch JL, Henderson E, Knopp MV, Larsson HB, ET AL. Estimating kinetic parameters from dynamic contrast-enhanced T(1)-weighted MRI of a diffusable tracer: Standardized quantities and symbols. *J Magn Reson Imaging* 1999;10:223-232. [https://doi.org/10.1002/\(SICI\)1522-2586\(199909\)10:3<223::AID-JMRI2>3.0.CO;2-S](https://doi.org/10.1002/(SICI)1522-2586(199909)10:3<223::AID-JMRI2>3.0.CO;2-S)
35. Buckley DL. Uncertainty in the analysis of tracer kinetics using dynamic contrast-enhanced T1-weighted MRI. *Magn Reson Med* 2002;47:601-606. <https://doi.org/10.1002/mrm.10080>
36. Ashton E, McShane T, Evelhoch J. Inter-operator variability in perfusion assessment of tumors in MRI using automated AIF detection. *Med Image Comput Comput Assist Interv* 2005;8:451-458. [https://doi.org/10.1007/11566465\\_56](https://doi.org/10.1007/11566465_56)
37. Lavini C, Verhoeff JJC. Reproducibility of the gadolinium concentration measurements and of the fitting parameters of the vascular input function in the superior sagittal sinus in a patient population. *Magn Reson Imaging* 2010;28:1420-1430. <https://doi.org/10.1016/j.mri.2010.06.017>
38. Keil VC, Mädler B, Gieseke J, Fimmers R, Hattingen E, Schild HH, Hadizadeh DR. Effects of arterial input function selection on kinetic parameters in brain dynamic contrast-enhanced MRI. *Magn Reson Imaging* 2017;40:83-90. <https://doi.org/10.1016/j.mri.2017.04.006>

39. Kim H, Mousa M, Schexnailder P, Hergenrother R, Bolding M, Ntsikoussalabongui B, Thomas V, Morgan DE. Portable perfusion phantom for quantitative DCE-MRI of the abdomen. *Med Phys* 2017;44:5198-5209. <https://doi.org/10.1002/mp.12466>
  40. Huang W, Li X, Chen Y, Li X, Chang MC, Oborski MJ, Malyarenko DI, ET AL. Variations of dynamic contrast-enhanced magnetic resonance imaging in evaluation of breast cancer therapy response: A multicenter data analysis challenge. *Transl Oncol* 2014;7:153-166. <https://doi.org/10.1593/tlo.13838>
  41. Guo Y, Zhu Y, Lingala SG, Lebel RM, Shiroishi M, Law M, Nayak K. High-resolution whole-brain dynamic contrast-enhanced MRI using compressed sensing. In: *Biomedical Optics & Medical Imaging*. SPIE Newsroom, 2015. <https://doi.org/10.1117/2.1201507.006016>
  42. Inglese M, Ordidge KL, Honeyfield L, Barwick TD, Aboagye EO, Waldman AD, Grech-Sollars M. Reliability of dynamic contrast-enhanced magnetic resonance imaging data in primary brain tumours: a comparison of Tofts and shutter speed models. *Neuroradiology* 2019;61:1375-1386. <https://doi.org/10.1007/s00234-019-02265-2>
  43. Morabito R, Alafaci C, Pergolizzi S, Pontoriero A, Iati G, Bonanno L, Gaeta M, Salpietro FM, Mormina E, Longo M, Granata F. DCE and DSC perfusion MRI diagnostic accuracy in the follow-up of primary and metastatic intra-axial brain tumors treated by radiosurgery with cyberknife. *Radiat Oncol* 2019;14:1-9. <https://doi.org/10.1186/s13014-019-1271-7>
  44. Tofts PS. Modeling tracer kinetics in dynamic Gd-DTPA MR imaging. *J Magn Reson Imaging* 1997;7:91-101. <https://doi.org/10.1002/jmri.1880070113>
  45. Barnes SR, Ng TSC, Santa-Maria N, Montagne A, Zlokovic BV, Jacobs RE. ROCKETSHIP: A flexible and modular software tool for the planning, processing and analysis of dynamic MRI studies. *BMC Med Imaging* 2015;15:19. <https://doi.org/10.1186/s12880-015-0062-3>
  46. Villringer K, Grittner U, Brunecker P, Khalil AA. DCE-MRI blood - brain barrier assessment in acute ischemic stroke. *Neurology* 2017;88:433-440. <https://doi.org/10.1212/WNL.0000000000003566>
  47. Tofts P. T1-weighted DCE Imaging Concepts: Modelling, Acquisition and Analysis. *Signal* 2010;500:400.
  48. Donaldson SB, West CML, Davidson SE, Carrington BM, Hutchison G, Jones AP, Sourbron SP, Buckley DL. A comparison of tracer kinetic models for T1-weighted dynamic contrast-enhanced MRI: Application in carcinoma of the cervix. *Magn Reson Med* 2010;63:691-700. <https://doi.org/10.1002/mrm.22217>
  49. Syková E, Nicholson C. Diffusion in brain extracellular space. *Physiol Rev* 2008;88:1277-1340. <https://doi.org/10.1152/physrev.00027.2007>
-